Applied Catalysis B: Environmental 188 (2016) 245–252

Contents lists available at ScienceDirect

Applied Catalysis B: Environmental

journal homepage: www.elsevier.com/locate/apcatb

Direct evidence of plasmonic enhancement on catalytic reduction of 4-nitrophenol over silver nanoparticles supported on flexible fibrous networks

Shuang Gao, Zhenyi Zhang*, Kuichao Liu, Bin Dong*

Key Laboratory of New Energy and Rare Earth Resource Utilization of State Ethnic Affairs Commission, School of Physics and Materials Engineering, Dalian Nationalities University, 18 Liaohe West Road, Dalian 116600, PR China

ARTICLE INFO

Article history:
Received 5 December 2015
Received in revised form 25 January 2016
Accepted 30 January 2016
Available online 8 February 2016

Keywords:
Electrospinning
Surface plasmon resonance
Silver nanoparticles
Flexible catalyst
Catalytic reduction

ABSTRACT

Direct evidence of plasmon-enhanced 4-nitrophenol (4-NP) reduction is observed in a photo-assisted catalytic process with the $NaBH_4$ as the electron donator by using the Ag nanoparticles (AgNPs) supported onto a flexible and processable polyacrylonitrile (PAN) microfibrous network. The Ag/PAN composite fibrous networks exhibit certain activity for 4-NP reduction in general condition. Significantly, when the beam irradiation is introduced to excite the surface plasmon resonance (SPR) of AgNPs, we observed an enhanced catalytic activity for 4-NP reduction (1 ~ 3 times). Meanwhile, the enhancement factors for the catalytic kinetic constants are directly correlated with the SPR absorption spectra of AgNPs. Further in-depth studies by adjusting the experiment conditions reveal that the SPR-induced ultrafast thermal effect of AgNPs is responsible for the enhanced catalytic activity that can not be nevertheless initiated or magnified by the hot plasmonic electrons from Ag. By combining with the theoretical analyses, we propose that this plasmon enhancement is ascribed to the promoted diffusion rate of reactants in the solution driven by increasing the local temperature around the AgNPs on the basis of SPR-enhanced electric field. Our present work provides a new sight to understand the plasmonic enhancement of metal-related catalytic reactions, and would also create more opportunities to guide the design and fabrication of high-performance plasmonic catalysts with excellent recycling property.

1. Introduction

Over the past decade, noble metal nanostructures with the advanced physical and chemical characteristics have attracted significant attention in the fields of electronics, photonics, biology, as well as catalysis [1–3]. Among various kinds of noble metal, the low-cost silver nanoparticles (AgNPs) are particularly interesting because their sizes and shapes can be optionally tailored for the purpose of modulating the electron configuration, leading to the improvement of their performance in the relevant applications [4–6]. In the case of reduction reactions catalyzed by Ag, the smaller AgNP usually shows the higher activity, since its higher surface-to-volume ratio and more negative redox potential are beneficial to the electrons transfer from Ag surface to reactants [7,8]. A central problem for using the small-sized AgNPs as catalysts is the aggregation phenomenon causing by their higher surface energies, which could minimize the surface area of catalysts [9,10]. The traditional method to overcome this drawback is the dispersion of AgNPs into some colloidal solutions to lower down their surface energy [11,12]. However, this treatment would cause loss in the catalytic activities due to the passivated surface-active sites of AgNPs. Meanwhile, the high-dispersed AgNPs are hardly to separate totally from the reaction solution, which therefore result in a poor performance for catalysts recycling [13,14]. From the above points of view, the immobilization of AgNPs onto a processable macro-support with the hierarchical nanostructures is a promising strategy to achieve both the high catalytic activity and excellent reusability simultaneously [15–17]. However, how to further enhance the catalytic capacity of these supported AgNPs is still a bottleneck that needs to be addressed urgently.

As is well known, the noble metal nanostructures also exhibit strong light absorption behavior due to the surface plasmon resonance (SPR) derived from the collective oscillation of surface electrons. Meanwhile, this fascinating optical characteristic has been widely employed as an energy/electron sensitization

* Corresponding authors.
E-mail addresses: zhangzy@dlnu.edu.cn (Z. Zhang), dong@dlnu.edu.cn (B. Dong).

http://dx.doi.org/10.1016/j.apcatb.2016.01.074
0926-3373/

channel to boost the related catalytic reaction, such as photocatalysis, photoelectricity, photochemistry, as well as catalytic reduction reaction [18–21]. Herein, in this work, we present a direct evidence to demonstrate plasmonic enhancement on the catalytic reduction of 4-nitrophenol (4-NP) to 4-aminophenol (4-AP) over AgNPs/polyacrylonitrile composite fibrous-networks (Ag/PAN CFN) in the presence of $NaBH_4$ as the electrons donator. The CFNs with controllable sizes and coverage densities of AgNPs were strategically synthesized through hydrothermal growth of the AgNPs onto PAN electrospun fibers-network, in which the PAN FN was used as the support to boost the functionalization of metal catalysts due to its flexibility, processability, as well as 3D open structure [22,23]. Furthermore, the 4-NP reduction reaction is the catalytic model of choice for the reactivity investigation, since this is an effective and classical process to evaluate the catalytic efficiency of metal NPs [24,25]. Not only that, the product of 4-AP is a multipurpose material that has been widely applied to manufacturing of photographic developer, hair-dyeing agent, analgesic, anti-pyretic, anticorrosion-lubricant, and so forth [26,27]. In this work, the as-synthesized Ag/PAN CFNs show certain catalytic activities for 4-NP reduction at room temperature without light irradiation. Significantly, when an irradiation beam at 450 ± 15 nm is introduced to excite the SPR of AgNPs, we observed $1.2 \sim 1.3$ times higher kinetic constants for 4-NP reduction, suggesting the improved catalytic activities. Further investigations by finely adjusting the incident wavelengths indicate that the enhancement factors on catalytic kinetic constant for the 4-NP reduction is directly correlated with the plasmonic absorption of AgNPs supported on the PAN microfibers. The control experiments operated at special parameter conditions suggest that the SPR-induced ultrafast photothermal effect is responsible to the promoted catalytic activity that can not be nevertheless initiated by the plasmonic hot electrons of AgNPs.

2. Experimental

2.1. Synthesis of Ag/PAN CFNs

1.2 g of polyacrylonitrile (PAN) powder was added into 10 mL of *N*,*N*-dimethylformamide slowly under stirring for overnight at room temperature to obtain the precursor. Then, the above precursor was transferred into a plastic syringe for electrospinning under the voltage of 10 kv. The products was collected at a distance about 12 cm to the syringe tip. Thus, the pure PAN fibrous network (FN) was formed through weaving the PAN electrospun microfibers. After that, 0.5 g glucose was dissolved in X (X = 36, 32, 30, 28) mL of deionized water under stirring for about 10 min at room temperature. Afterwards, 10 mg of the as-electrospun PAN FN was added into the glucose solution and stirred for about one hour at room temperature. Then, an appropriate amount (40-X) mL of $Ag(NH_3)_2OH$ aqueous solution (0.02 M) was dropped into the above mixture solution. At last, this mixture solution was transferred into a 50 mL teflon-lined stainless steel autoclave to implement the hydrothermal process at 160 °C for 3 h. When the autoclave was cooled down to room temperature, the obtained Ag/PAN CFNs were washed with deionized water and ethanol to remove any ionic residue, then dried in an oven at 60 °C for 12 h. In order to control the sizes and coverage densities of AgNPs on the PAN microfibers surface, 4, 8, 10, and 12 mL of $Ag(NH_3)_2OH$ aqueous solution (0.02 M) were dropped into the hydrothermal precursor solution to produce the Ag/PAN CFNs denoted as Ag/PAN CFN-1, Ag/PAN CFN-2, Ag/PAN CFN-3, Ag/PAN CFN-4, respectively.

2.2. Catalytic reduction of 4-NP

1.75 g NaOH was added to 250 mL of 0.13 mM 4-NP aqueous solution. And then, 10 mg of the as-synthesized Ag/PAN CFN catalysts were added to 30 mL of the above 4-NP aqueous solution. Subsequently, the above solution was mixed with 30 mL fresh $NaBH_4$ solution (88 mM). The reaction was carried out at room temperature in the nitrogen atmosphere. Reduction reaction process was monitored by recording the UV–vis absorption spectra of the reaction solution at appropriate time intervals during the reaction. A 300W Xe lamp (PLS-SXE300UV) coupled with different bandpass filters were used as the light sources to irradiate the samples during the catalytic reactions, in which the light intensities of 420 ± 15, 450 ± 15, 475 ± 15, and 500 ± 15 nm were 160, 100, 85, and 65 mw/cm^2, respectively.

2.3. Characterization

X-ray diffraction (XRD) patterns of the as-synthesized samples were measured by a Shimadzu XRD-6000 X-ray diffractometer with a Cu Kα line of 0.1541 nm. Scanning electron microscopy (SEM; XL-30 ESEM FEG, Micro FEI Philips) and transmission electron microscopy (TEM; JEOL JEM-2100) were employed to observe the morphologies and structures of the samples. X-ray photoelectron spectroscopy (XPS) was carried out on a VG-ESCALAB LKII instrument with a Mg Kα ADES ($h\nu = 1253.6$ eV) source at a residual gas pressure below 10^{-8} Pa. Thermal gravimetric and differential thermal analysis (TG-DTA) was carried out on a NETZSCH STA 449C thermo-analyzer in air. Raman spectra were collected by Renishaw inVia Raman Microscope using the 532 nm laser as the excitation source. Fourier transform infrared (FT-IR) spectra were recorded on a Magna 560 FT-IR spectrometer with a resolution of 1 cm^{-1}. UV–vis absorption spectra were taken with a Lambda 750 UV/Vis/NIR spectrophotometer (Perkin Elmer, USA).

3. Results and discussion

To achieve the ideal structure of Ag/PAN CFN, a two-step synthesis route was adopted in our work (Fig. 1A). In the first step, the PAN microfibrous network as a tailorable substrate was fabricated in macroscopic scale through a facile electrospinning technique. For the second step, the nanosized Ag particles were immobilized onto the as-electrospun PAN microfiber surfaces by a traditional hydrothermal method to construct the micro/nano- hierarchical heterostructural CFNs. By appropriately adjusting the hydrothermal parameter, the size and coverage density of Ag NP could be controlled to systematic investigation of the relationship between microstructures and catalytic activities of the Ag/PAN CFNs. As shown the scanning electron microscopy (SEM) image in Fig. 1B, the pure PAN electrospun fibers with diameters of $1.0 \sim 1.3$ μm show smooth surface due to the amorphous nature of polymer PAN. After hydrothermal treatment, a large number of spherical particles with the mean size of ~57 nm appear on the surface of PAN microfibers (Fig. 1C). Further observation under the transmission electron microscopy (TEM) indicates the different spacing between the adjacent NPs, resulting in the formation of dimer-, trimer-, or even multimer-like nanostructures on the PAN microfiber surface (Fig. 1D). Moreover, there are also many AgNPs-aggregations in the Ag/PAN CFN, which reduces the exposed area of AgNPs and therefore may show a lower catalytic activity. The selected area electron diffraction (SAED) pattern of an individual Ag/PAN CFN reveals the existence of polycrystalline AgNPs with face centered cubic (fcc) structure (Fig. 1E). The representative high resolution TEM (HRTEM) image taken from the single NP on the products shows the well resolved (111) lattice fringes (d = 0.235 nm) of fcc

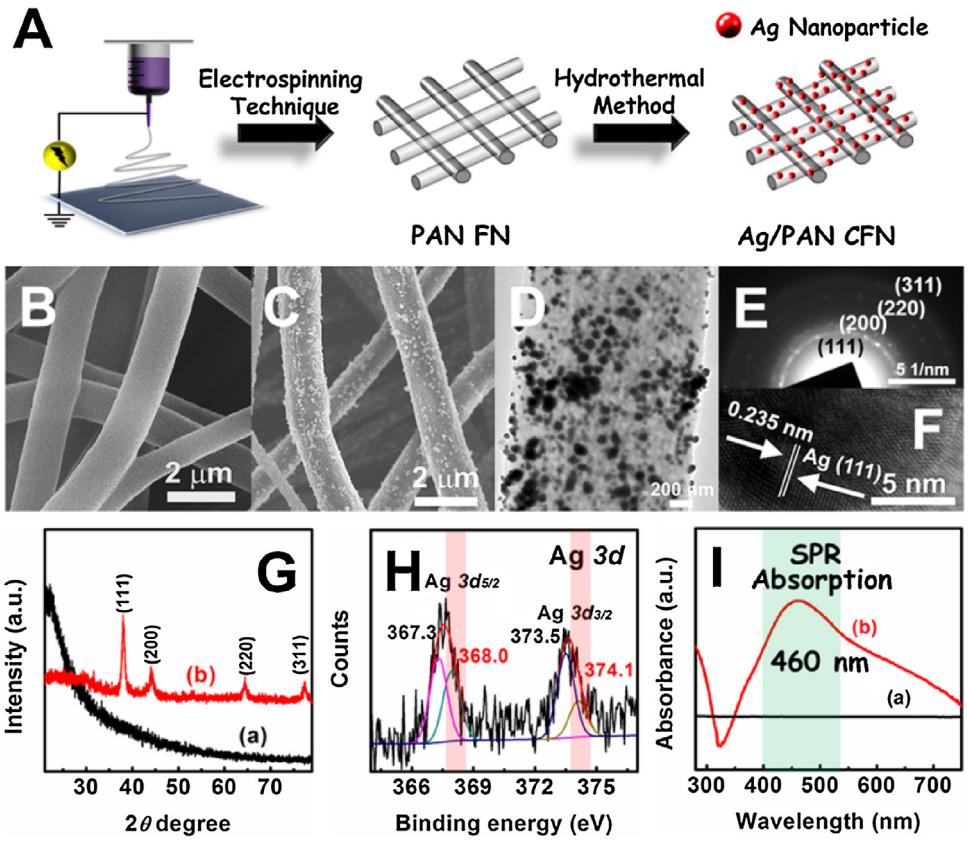

Fig 1. (A) Synthesis route of the Ag/PAN CFNs; SEM images of (B) pure PAN microfibers and (C) Ag/PAN composite microfibers; (D) TEM image and (E) the corresponding SAED pattern of an individual Ag/PAN composite microfiber; (F) HRTEM image of the AgNP supported on the PAN microfibers; (G) XRD patterns of (a) PAN FN and (b) Ag/PAN CFN-3; (H) XPS spectrum of Ag *3d* core-level; (I) UV–vis absorption spectra of (a) PAN FN and (b) Ag/PAN CFN-3.

Ag characteristics, further revealing that the NPs supported on the PAN microfibers are fcc metallic Ag (Fig. 1F). In comparison with the X-ray diffraction (XRD) pattern of PAN microfibrous network that only shows a polymer semicrystalline band around 22°, the Ag/PAN CFN displays four sharp diffraction peaks originated from the fcc structure of Ag (Fig. 1G). It suggests the formation of metallic Ag/polymer PAN composite. However, the X-ray photoelectron spectroscopy (XPS) analysis implies that, besides the zero-valent metallic Ag with the binding energies at 368.0 eV (Ag $3d_{5/2}$) and 374.1 eV (Ag $3d_{3/2}$), a large amount of oxidation state can be found on the surface of AgNPs (367.3 eV for Ag $3d_{5/2}$ and 373.5 eV for Ag $3d_{3/2}$) (Fig. 1H) [28], which may influence on the induction time during the 4-NP catalytic reduction. As shown in Fig. 1I, the Ag/PAN CFN exhibits an obvious absorption band peaked at ~460 nm which can be ascribed to the surface plasmon resonance (SPR) of supported AgNPs [8,14]. However, this feature absorption peak can not be observed on the absorption curve of pure PAN FN.

In order to provide more flexible CFNs for the optimization of the AgNPs-based catalysts, a series of CFNs with the AgNPs content of 7.0 wt.%, 15.0 wt.%, 20.0 wt.% and 30.0 wt.% were synthesized and denoted as the Ag/PAN CFN-X, X = 1, 2, 3, 4, respectively (Fig. S1). The amount of AgNPs in the as-synthesized CFNs was estimated by the thermal gravimetric analysis (TGA). Meanwhile, the interactions between the AgNPs and PAN could be reflected on the differential thermal analysis (DTA) curves, on which the more AgNPs on the PAN microfiber surface, the more obvious the interactions it shows (Fig. S2). As expected, the microstructure and optical property of the as-synthesized CFNs are strongly dependent on the Ag content. With increasing of the Ag content from 7.0 wt.%, to 30.0 wt.%, the mean sizes of AgNPs are enlarged from 48 to 63 nm (Fig. 2A and Fig. S3), accompanied by the red-shift of SPR absorption peak of AgNPs from 440 to 475 nm (Fig. 2A and Fig. S4). The Fourier transform infrared (FT-IR) spectra shown in Fig. 2B present that, after hydrothermal growth of AgNPs onto the PAN microfibers surface, the relative intensity of stretching vibration band related to the C=N of PAN (2245 cm^{-1}) is slightly weakened as compared to the pure PAN microfibers [29]. It implies that a small quantity of C=N group on PAN microfibers surface may interact with the metal Ag during the high-temperature reaction, thereby deforming the chemical structure of C=N group.

This interaction can be understood more clearly through Raman spectra analyses. In Fig. 2C, there is no Raman signal on the curve of pure PAN FN. However, in the case of Ag/PAN CFNs, two broad overlapping peaks with the center at 1360 cm^{-1} and 1580 cm^{-1} appear on the Raman spectra (Fig. S5), which are consistent with the peak positions of aromatic ring structure of graphitic carbon, and are usually labeled as D peak indicated the defects of SP^3 carbon and G peak suggested the SP^2 graphite carbon, respectively [30]. Generally, the integrated intensity ratio of D to G peak, denoted by $R = I_D/I_G$, reveals the degree of cyclization (or graphite mole fraction) of carbon-based materials [31]. As shown in Fig. 2D, the R values are increased gradually with the increased content of AgNPs in the Ag/PAN CFNs, suggesting that the interaction between the Ag and PAN is more obvious when more AgNPs supported onto the PAN microfibers surface to react with them. This phenomenon is in agreement with that concluded by DTA results, revealing that the aromatic ring structure is built up to the metal AgNPs surface through linking with the N atoms or at least that the fused rings are sticking up to the surface [32,33], as illustrated in the inset of Fig. 2D. Thus, the metal-induced cyclization on Ag/PAN system induces a strong Raman signal similar to that observed on the aromatic ring structure of graphitic carbon. However, the corresponding vibra-

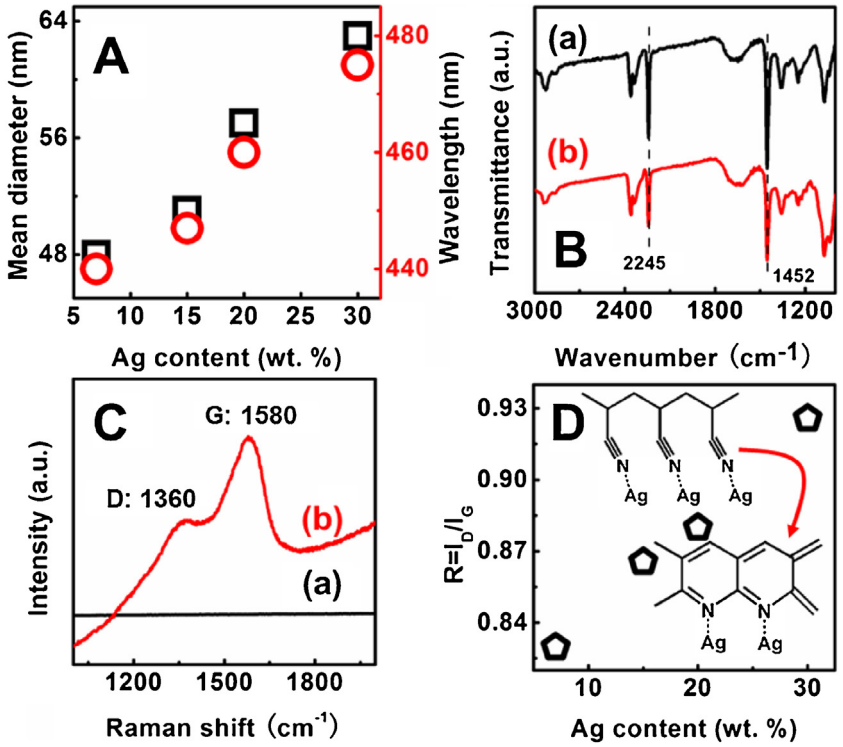

Fig. 2. (A) Mean diameters of the loaded AgNPs and UV–vis absorption peaks of Ag/PAN CFNs versus Ag content in the different Ag/PAN CFNs; (B) FT-IR spectra of (a) PAN FN and (b) Ag/PAN CFN-3; (C) Raman spectra of (a) PAN FN and (b) Ag/PAN CFN-3; (D) integrated intensity ratio of D to G peak for Ag/PAN CNs with different Ag content; the inset showing the scheme of cyclization process of PAN after hydrothermal growth of AgNPs.

tion signals could not be caught on the curve of FT-IR spectra due to their very low content beyond the detection limit.

The catalytic activities of the as-synthesized Ag/PAN CFNs were investigated through the reduction of 4-NP to 4-AP with an excess amount of $NaBH_4$. All the catalytic reactions were performed in aqueous solution without magnetic stir. In general, the 4-NP aqueous solution shows a strong absorption peak at 317 nm in acidic or neutral conditions. After the addition of $NaBH_4$, the absorption peak of 4-NP red-shifts from 317 to 400 nm immediately, accompanied with the color change from light yellow to yellow-green because of the formation of 4-nitrophenolate ions [25,34]. However, there were no changes occurring on both the solution color and absorption spectra even after prolonging the time for 3 h (Fig. S6A), indicating that the reduction reaction can not be initiated in the absence of metal catalysts due to the kinetic barrier between the mutually repelling negative ions 4-NP and BH_4^- [35]. Accordingly, we did not observe any absorption peak relating to the reducing product of 4-AP when using the pure PAN CFN as the catalyst (Fig. S6B). Notably, after adding the as-synthesized Ag/PAN CFNs into the reaction solution, the yellow-green color from the 4-nitrophenolate ions diminished after a period of time. Correspondingly, its feature absorption peak centered at 400 nm also decreased, while a new absorption peak attributed to 4-AP begin to rise as a shoulder at 295 nm (Fig. 3A). These observations demonstrate the reduction of 4-NP to produce the 4-AP by the metal AgNPs supported on the PAN FNs. Note that there exist an induction period during which no trace of absorption signal belonging to the catalytic product of 4-AP were observed. Such induction period can sustain 10 ~ 30 min in our case and is inversely proportional to the AgNPs content on the PAN FNs (Fig. S7). This process can be explained by two main reasons based on the previous results: (1) the poor diffusion behavior of 4-NP in the absence of magnetic stir [36]; (2) the existence of oxidation state on the AgNPs surface as evidenced by XPS result [37,38]. Thus, the reduction of oxidation state on the AgNPs surface by the borohydride should take place in the induction period, which is also a premise to ensure the catalytic reduction of 4-NP on Ag surface. As shown in Fig. 3A, after this induction period, the reduction reaction takes place along with the production of 4-AP. Note that when the catalytic reaction was carried out under vigorous stirring, the induction period could be shorten and the catalytic kinetic constant was increased accordingly (Fig. S8). This indicates that after improving diffusion behavior of 4-NP by magnetic stir, the contact between the AgNPs and reaction reagents (4-NP and $NaBH_4$) could be greatly promoted, therefore increasing the rate of electron transfer from $NaBH_4$ to AgNPs, and to 4-NP for enhancing the reduction process.

In order to compare the catalytic activities of the different Ag/PAN CFNs on the reduction of 4-NP, the kinetics behaviors for the catalytic reactions were monitored through recording the absorbance of 4-nitrophenolate ions. As an excess of $NaBH_4$ was added to provide the reducibility during the catalytic reaction, the first approximation could be chose to calculate the kinetics data based on a pseudo-first-order rate law. The apparent rate constant (k_{app}) is proportional to the surface area of metal NPs, which could be defined as follow [36,24]:

$$-\frac{dC}{dt} = k_{app}C = k_1SC$$

where C is 4-NP concentration at time (t); k_1 is the rate constant normalized to S, the surface area normalized to the unit volume of catalysts. For each case, the linear correlation can be observed between $\ln(C/C_0)$ and real reaction time (after the induction period). Correspondingly, the k_{app} values were obtained from the slopes of above plots and summarized in the inset of Fig. 3B. It means that the catalytic activity of Ag/PAN CFN is gradually enhanced with the increase of Ag content due to the increased catalytic sites on the PAN microfibers. However, when the Ag content reaches 30.0 wt.%, a rapid reduction in the catalytic activity

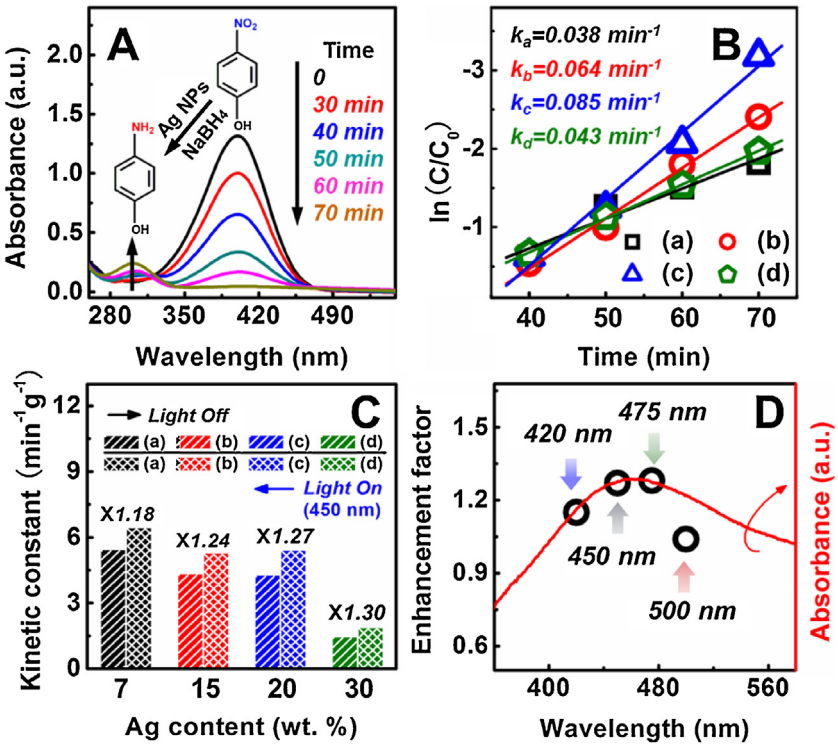

Fig. 3. (A) UV–vis absorption spectra during the catalytic reduction of 4-NP over Ag/PAN CFN-3; (B) $\ln(C/C_0)$ versus reaction time (after induction period) for the 4-NP catalytic reduction over the different Ag/PAN CFNs (C_0 and C are the absorption peak at 400 nm initially and at reaction time *t*, respectively); (C) kinetic constants of the 4-NP catalytic reduction over the as-synthesized Ag/PAN CFNs with and without 450 ± 15 nm irradiation; (D) wavelength-dependent enhancement factors for the kinetic constants of 4-NP catalytic reduction at room temperature over the Ag/PAN CFN-3.

is observed. This decrease may be ascribed to the existence of many aggregations of AgNPs (see Fig. S3), leading to minimizing the potential active sites.

When normalized with the mass content of Ag, the rate constants on a per gram Ag basis (k_{Ag}) show an obvious declining trend from Ag/PAN CFN-1 to Ag/PAN CFN-4 (Table S1). This observation could be understood by the size-dependent catalytic property of noble metal NPs. In the morphology point of view, the NP with smaller size possesses the larger surface-to-volume ratio and more active sites for catalysis [39]. This traditional explanation is in accordance with the results obtained in our work. Besides, from the aspect of internal energy-band structure, the potential barrier built at the interface between AgNP and 4-NP (−0.76 V vs. NHE) is also the key point that affects the catalytic activity of AgNP [8]. The redox potential E_p of AgNP can be estimated according to the following equation [6,40]:

$$E_p = \left(E_{Bulk} - \frac{2\gamma v_M}{zFr}\right)$$

where $E_{Bulk} = +0.8V$ (vs. NHE) is the redox potential of Ag bulk material; $\gamma = 1.45 J cm^{-2}$ is the surface tension; z is the lowest valence state; v_M is the molar volume; F is Faraday's constant; r is the radius of AgNP. Obviously, E_p are +0.774 V for 48 nm AgNP, +0.776 V for 51 nm AgNP, +0.778 V for 57 nm AgNP, and +0.780 V for 63 nm AgNP. Accordingly, the potential barrier heights between the AgNP and 4-NP are about 1.534 V for Ag/PAN CFN-1, 1.536 V for Ag/PAN CFN-2, 1.538 V for Ag/PAN CFN-3, and 1.540 V for Ag/PAN CFN-4. It is easy to conclude that the small sized AgNP presents a low potential barrier and higher surface area, which can synergistically boost the electron transfer process from AgNP surface to reactant 4-NP in the presence of highly injecting electron from the donator of BH_4^- ions, and therefore promote the catalytic reduction activity.

To our surprise, when we introduced a light beam with the wavelength at 450 ± 15 nm to irradiate the Ag/PAN CFNs during the catalytic reduction process, the kinetic constants were distinctly increased, meaning the enhanced catalytic activities of AgNPs supported on PAN CFs (Fig. 3C). Since the excitation wavelength is in the region of AgNPs absorption, it is proposed that the SPR effect of AgNPs may play a certain role on the enhancement of catalytic ability. In order to clarify this assumption, we preformed the comparison experiment on Ag/PAN CFN through finely controlling the irradiation wavelengths at 420 ± 15, 450 ± 15, 475 ± 15, and 500 ± 15 nm, respectively. These wavelengths are selected according to the AgNPs SPR band in the absorption spectrum. As observed in Fig. 3D, the enhancement factors, denoting the ratio values of kinetic constants measured under light irradiation to these obtained in dark, exhibit strong dependence on the irradiation wavelength which are in agreement with the plasmon absorption band of AgNPs in the Ag/PAN-3CFN. The irradiation at 475 ± 10 nm contributes the highest enhancement factor (1.28x) on the catalytic reduction of 4-NP (Fig. S9A). These results provide the solid proof that the SPR excitation of AgNPs is the dominating factor responsible for the enhanced catalytic activity of Ag/PAN CFNs. Moreover, it is of great significance to note that the SPR-induced enhancement on the catalytic activity is slightly decreased from Ag/PAN CFN-4 to Ag/PAN CFN-1 (Fig. 3C and Fig. S9B), which implies that the size and distribution of AgNPs on the PAN FNs also influence the SPR effect. Firstly, the plasmonic NPs with a larger size usually show a stronger SPR-induced localized electric field surrounding their surface [41,42]. Secondly, the adjacent (or attached) plasmonic NPs in the aggregation may construct the unique plasmonic nanostructure, such as dimer-, trimer-, or even multimer-like nanostructure, which can induce a great enhancement on the localized electric field in the special region among the noble metal NPs under the SPR-excitation [43,44]. Thus, the large sized AgNPs with high

density on the PAN FN should display the higher catalytic activity based on the SPR effect. This phenomenon indirectly confirms that the reduction of 4-NP to 4-AP catalyzed by AgNPs can be further enhanced through exciting the collective oscillation of surface electrons for plasmonic NPs.

On the other hand, upon the plasmon excitation, the "hot" electrons around the Fermi level of plasmonic nanostructure might reach a virtual high-energy state, and then inject to the nearby acceptor to fulfill the (photoelectro-) photo-chemical reactions. The SPR-induced direct electron transfer process has been supported by ultrafast spectroscopic studies and widely applied in the fields of photoelectrochemical cell and photocatalysis [18–20,41,42]. However, we found that the individual irradiation at 420 ± 15, or 450 ± 15, or 475 ± 15, or 500 ± 15 nm could not result in observable 4-AP production in the absence of $NaBH_4$ as the electrons injector. This suggests that the hot plasmon electrons are not able lead to the 4-NP reduction on AgNP surface under the present reaction condition, thus the SPR-driven hot electron could not transfer to the 4-NP and contribute to the enhanced catalytic property, possibly owing to the short lifetime of plasmon electrons and large overpotential of 4-NP reduction on AgNP. However, further investigations found that, when an irradiation beam with the wavelength at 475 ± 10 nm was implemented in the classical model reaction of 4-NP catalytic reduction, the reaction solution temperature could reach ~35 °C after 40 min. This value is higher than that obtained in the absence of either light irradiation (~27 °C) or CFNs catalysts (~30 °C), suggesting that the SPR excitation of AgNPs may induce the thermal effect during the catalytic reduction reaction. According to the Arrhenius equation [25]:

$$k = Ae^{\frac{-E_a}{RT}}$$

where A is the frequency factor; E_a is the activation energy; T is the circumstance temperature. Thus, if the activation energy is a constant value for the AgNPs in the used catalyst, the kinetic constant should be proportional to the temperature of reaction solution. This is to say, the enhanced catalytic activity of Ag/PAN CFNs is mainly due to the improvement of reaction kinetic process on 4-NP reduction by the SPR-excited thermal effect.

The photothermal effect driven by the SPR-excitation of plasmonic metal nanostructure has been widely studied during the past decade [45,46]. Upon the plasmon excitation, the surface electrons of metal can be rapidly heated to high temperature (several hundreds of degree), then relax within a short time to release phonon energy which transfer radially from the metal surface [46]. As such, a temperature gradient would be formed surrounding the plasmonic metal. Furthermore, the relaxation time of heat dissipation for the excited-plasmonic nanostructure in aqueous solution is very short (~10^{-9} s) [46–48]. As a result of a low thermal diffusivity for water (~10^{-7} m^2 s^{-1}), the photogenerated transient heat is difficult to accumulate for significantly enhancing the temperature of reaction solution. Thus, only several degree of temperature increase was observed after introducing the irradiation beam to initiate the photothermal effect in the catalytic reduction reaction. Although the real temperature driven by the photothermal effect is hardly detected by using the general method, it can be expressed through the theoretical equation described as follow [46,49]:

$$Q_d = \frac{1}{2}\varepsilon_0 \omega \mathrm{Im}(\varepsilon_r)|\boldsymbol{E}|^2$$

where Q_d is the heat power volume density; ω is the angular frequency of the light; ε_0 and ε_r are the permittivity of vacuum and the relative permittivity of metal, respectively; E is the electric field. It is clearly that the heat generation is partly determined by the electric field nearby the metal NPs that can be locally amplified through the plasmon excitation as aforementioned mentioned. These analyses suggest that the excitation of AgNPs SPR might greatly increase the localized temperature surrounding the AgNPs surface through enhanced electric field so that the kinetic process of electron transport on Ag surface is boosted in the catalytic reduction reaction.

If this is true, the enhancement factor should be related with the temperature change around the AgNPs. In order to clarify this viewpoint, we carried out another series of control experiments, in which the reaction temperature was lowered down to 0 °C through immersing the reactor into a vessel loaded with ice-water mixture. It is expected that a larger temperature increase would be realized nearby the AgNPs surface after introducing the SPR irradiation to implement the photothermal effect. As shown in Fig. 4A, in the absence of light irradiation, the Ag/PAN CFN-3 shows the longer induction period (50 min) and the smaller kinetic constant (0.012 min^{-1}) as compared to the corresponding values obtained at the room temperature. These results further demonstrate that the reaction temperature is an important parameter condition for influencing the catalytic activity of AgNPs. Interestingly, upon the excitation of AgNPs SPR, the kinetic constants of Ag/PAN CFN-3 catalyst are greatly enhanced with the maximum value of 0.036 min^{-1} obtained under 475 ± 15 nm irradiation. Meanwhile, the wavelength-dependent catalytic property was also observed on this SPR-excited catalytic system (Fig. 4B). Notably, the enhancement factors appeared in these control experiments are obviously higher than the corresponding values presented in Fig. 3D. It is implied that a larger temperature difference might be emerged in this catalytic system due to the SPR-induced photothermal effect. Unfortunately, owing to the ultrafast photothermal process and low thermal diffusivity of water, we only observed about 11.8 °C enhancement on the temperature by direct detection of the reaction solution during the SPR-excited catalytic reaction (irradiation for 40 min). Nevertheless, based on the above experiments and analyses, it is no less reasonable to believe that the effect of SPR excitation on inducing the photothermal process is the primary factor responsible for the enhanced catalytic activity of Ag/PAN CFN in the 4-NP reduction reaction.

In the case of 4-NP catalytic reduction, the electrons transfer on the AgNPs surface might be the essential problem to influence the kinetic constant or catalytic activity of catalyst, which should depend on the diffusion of 4-NP to the AgNPs surface and the diffusion of 4-AP away from their surface. In this way, the reaction rate constant could be also expressed as [50]:

$$\frac{1}{k_{Ag}} = \frac{1}{4\pi R^2}\left(\frac{1}{k_e} + \frac{R}{D}\right)$$

where R is the radius of the metal NP; k_e is the rate constant of electron transfer; D is the diffusion coefficient of solvent. When the heterogeneous charge transfer is much faster than the solute diffusion, the above formula can be simplified as the Smoluchowski equation [51,52]:

$$k_{Ag} = 4\pi DR$$

This expression also applies to our present catalytic system because of the strong driving force for the AgNPs-mediated electrons transfer in the presence of highly injecting electrons from BH_4^-. If we neglect the difference on the radii of the AgNPs in one CFN, the reaction rate of catalyst is mainly controlled by the 4-NP diffusion in the reaction solution. Actually, the diffusion coefficient of 4-NP can be expressed approximately through the Stokes-Einstein equation:

$$D = \frac{k_B T}{3\pi \beta_w \sigma_{4NP}}$$

where $\sigma_{4NP}$is the molecular radius of 4-NP;β_w is the solvent viscosity. It can be easily deduced that the diffusion coefficient of 4-NP increases with the raising of solution temperature. Likewise,

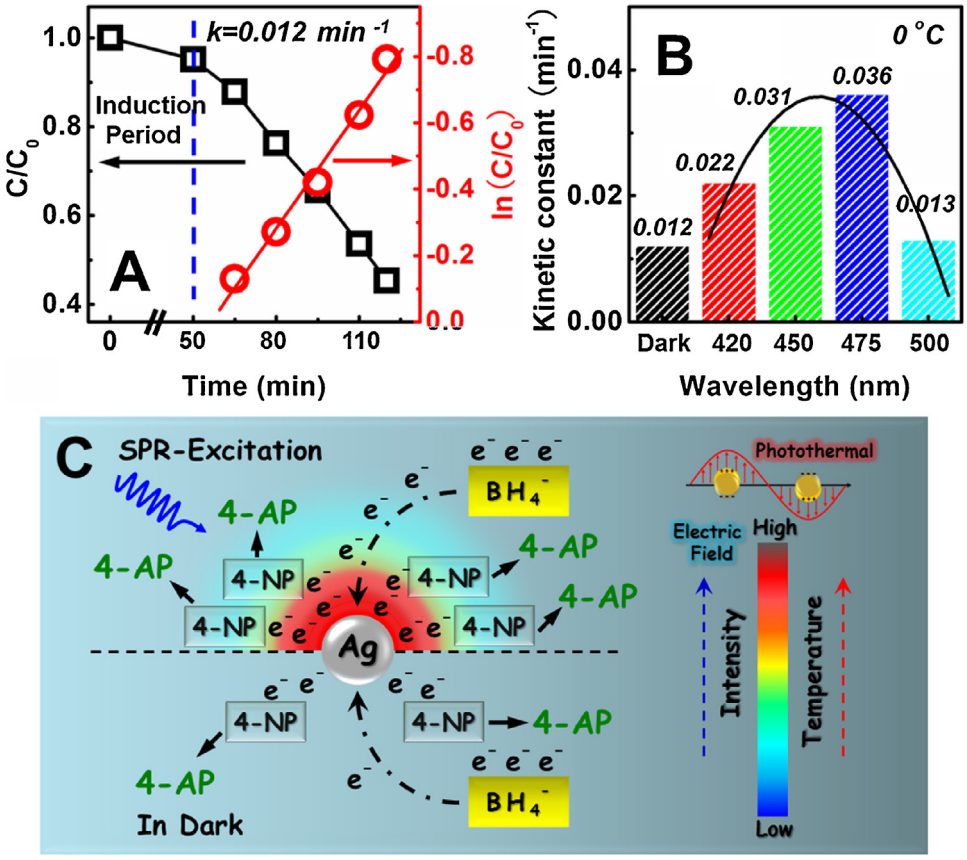

Fig. 4. (A) C/C_0 and $\ln(C/C_0)$ versus reaction time for the 4-NP catalytic reduction at 0 °C over the Ag/PAN CFN-3; (B) kinetic constants of the 4-NP catalytic reduction at 0 °C over Ag/PAN CFN-3 versus the irradiation wavelengths; (C) schematic diagram of SPR-excited thermal effect on the enhancement of 4-NP catalytic reduction over AgNPs supported on the PAN microfibers in the presence of highly electron injecting $NaBH_4$.

when the localized temperature is increased around AgNPs surface, the reduction product of 4-AP would be moved away from the AgNPs surface more quickly due to the enlarged diffusion coefficient. Thus, upon the SPR excitation on AgNPs supported on the PAN microfibers surface, the generated ultrafast thermal effect could greatly raise the localized temperature nearly AgNPs in the reaction solution based on the enhancement of localized electric field, by which the diffusivity of reactant 4-NP and product 4-AP could be significantly enhanced in the region around AgNPs surface, therefore promoting the catalytic activity of Ag/PAN CFN (Fig. 4C). Besides, this kind of organic/inorganic composite catalyst can be collected easily from the reaction solution without reducing the catalytic activity, indicating its excellent recycling property by taking the advantages of flexibility, tailorability, and unique hierarchical heterostructure (Fig. S10).

4. Conclusions

In conclusion, we have demonstrated direct evidence of plasmon enhancement of 4-NP catalytic reduction over size-controlled AgNPs supported onto electrospun PAN microfibrous networks in the presence of highly injecting electrons from $NaBH_4$. Further investigations found that the SPR-induced ultrafast thermal effect is responsible for the enhanced catalytic activity of Ag/PAN composite fibrous networks through boosting the reactants diffusion behavior nearby the catalyst surface on the basis of photothermal effect. However, the SPR-induced hot electrons on AgNPs surface could not directly fulfill the catalytic reaction on 4-NP reduction in the absence of $NaBH_4$ as the electron donator. Importantly, the present work offers a new insight to further promote the catalytic reduction activity of plasmonic NPs through the excitation of their intrinsic optical property. We believe that the photothermal effect may also exist and play key roles in other plasmonic metal-related reduction reactions under irradiation in a wide range of wavelengths that can initiate the metal SPR.

Acknowledgements

This work is supported by the National Natural Science Foundation of China (grant nos. 51402038, 11474046, and 11274057), Program for New Century Excellent Talents in University (NCET-13-0702), Technology Foundation for Selected Overseas Chinese Scholar from Ministry of Personnel of China, Scientific Research Foundation for Doctor of Liaoning Province (grant no. 20141118), Educational Committee Foundation of Liaoning Province (grant no. L2014547), Science and Technology Project of Liaoning Province (grant no. 2012222009), Program for Liaoning Excellent Talents in University (LNET) (grant no. LR2015016), Science and Technique Foundation of Dalian (grant no. 2014J11JH134 and 2015J12JH201), and Fundamental Research Funds for the Central Universities (grant nos. DC201502080203 and DC201502080304).

Appendix A. Supplementary data

Supplementary data associated with this article can be found, in the online version, at http://dx.doi.org/10.1016/j.apcatb.2016.01.074.

References

[1] S. Nie, S.R. Emory, Science 275 (1997) 1102–1106.
[2] K. Brandt, M.E. Chiu, D.J. Watson, M.S. Tikhov, R.M. Lambert, J. Am. Chem. Soc. 131 (2009) 17286–17290.
[3] M. Rycenga, C.M. Cobley, J. Zeng, W. Li, C.H. Moran, Q. Zhang, D. Qin, Y. Xia, Chem. Rev. 111 (2011) 3669–3712.
[4] J. Rosen, G.S. Hutchings, Q. Lu, S. Rivera, Y. Zhou, D.G. Vlachos, F. Jiao, D.G. Vlachos, F. Jiao, ACS Catal. 5 (2015) 4293–4299.
[5] D. Tsukamoto, A. Shiro, Y. Shiraishi, Y. Sugano, S. Ichikawa, S. Tanaka, T. Hirai, ACS Catal. 2 (2012) 599–603.
[6] P.L. Redmond, A.J. Hallock, L.E. Brus, Nano Lett. 5 (2005) 131–135.
[7] K. Mori, A. Kumami, M. Tomonari, H. Yamashita, J. Phys. Chem. C 113 (2009) 16850–16854.
[8] Z. Zhang, C. Shao, Y. Sun, J. Mu, M. Zhang, P. Zhang, Z. Guo, P. Liang, C. Wang, Y. Liu, J. Mater. Chem. 22 (2012) 1387–1395.
[9] M.V. Canamares, J.V. Garcia-Ramos, J.D. Gomez-Varga, C. Domingo, S. Sanchez-Cortes, Langmuir 21 (1) (2005) 8546–8553.
[10] H. Hu, J.H. Xin, H. Hu, X. Wang, D. Miao, Y. Liu, J. Mater. Chem. A 3 (2015) 11157–11182.
[11] X.F. Yang, A.Q. Wang, B.T. Qiao, J. Li, J.Y. Liu, T. Zhao, Acc. Chem. Res. 46 (2013) 1740–1748.
[12] C.-L. Zhang, S.-H. Yu, Chem. Soc. Rev. 43 (2014) 4423–4448.
[13] A.C. Patel, S. Li, C. Wang, W. Zhang, Y. Wei, Chem. Mater. 19 (2007) 1231–1238.
[14] P. Zhang, C. Shao, Z. Zhang, M. Zhang, J. Mu, Z. Guo, Y. Liu, Nanoscale 3 (2011) 3357–3363.
[15] M. Zhu, C. Wang, D. Meng, G. Diao, J. Mater. Chem. A 1 (2013) 2118–2125.
[16] X. Liu, R. Jin, D. Chen, L. Chen, S. Xing, H. Xing, Y. Xing, Z. Su, J. Mater. Chem. A 3 (2015) 4307–4313.
[17] Q. Mao, S. Shi, H. Wang, ACS Sustain. Chem. Eng. 3 (2015) 1915–1924.
[18] S. Linic, P. Christopher, D.B. Ingram, Nat. Mater. 10 (2011) 911–921.
[19] Z. Zhang, Y. Huang, K. Liu, L. Guo, Q. Yuan, B. Dong, Adv. Mater. 27 (2015) 5906–5914.
[20] X. Wang, C. Liow, A. Bisht, X. Liu, T.C. Sum, X. Chen, S. Li, Adv. Mater. 27 (2015) 2207–2214.
[21] M. Hajfathalian, K.D. Gilroy, A. Yaghoubzade, A. Sundar, T. Tan, R.A. Hughes, S. Neretina, J. Phys. Chem. C 119 (2015) 17308–17315.
[22] J. He, W. Wang, F. Sun, W. Shi, D. Qi, K. Wang, R. Shi, F. Cui, C. Wang, X. Chen, ACS Nano 9 (2015) 9292–9302.
[23] Z. Guo, C. Shao, J. Mu, M. Zhang, Z. Zhang, P. Zhang, B. Chen, Y. Liu, Catal. Commun. 12 (2011) 880–885.
[24] M. Schrinner, M. Ballauff, Y. Talmon, Y. Kauffmann, J. Thun, M. Moller, J. Breu, Science 323 (2009) 617–620.
[25] J. Zeng, Q. Zhang, J. Chen, Y. Xia, Nano Lett. 10 (2010) 30–35.
[26] C.V. Rode, M.J. Vaidya, R.V. Chaudhari, Org. Process Res. Dev. 3 (1999) 465–470.
[27] J.F. Corbett, Dyes Pigm. 41 (1999) 127–136.
[28] J.A. Toledo-Antonio, M.A. Cortes-Jacome, C. Angeles-Chavez, E. Lopez-Salinas, P. Quintana, Langmuir 25 (2009) 10195–10201.
[29] Z. Zhang, X. Li, C. Wang, S. Fu, Y. Liu, C. Shao, Macromol. Mater. Eng. 294 (2009) 673–678.
[30] Y. Wang, S. Serrano, J.J. Santiago-Avilés, Synth. Met. 138 (2003) 423–427.
[31] F. Tuinstra, J.L. Koenig, J. Chem. Phys. 53 (1970) 1126–1130.
[32] D.-S. Zhou, N. Xu, L. Li, G. Ji, G. Xue, J. Phys. Chem. B 107 (2003) 2748–2751.
[33] B.H. Loo, Y.G. Lee, D.O. Frazier, J. Phys. Chem. 89 (1985) 4672–4676.
[34] S. Saha, A. Pal, S. Kundu, S. Basu, T. Pal, Langmuir 26 (2010) 2885–2893.
[35] J. Huang, S. Vongehr, S. Tang, H. Lu, X. Meng, J. Phys. Chem. C 114 (2010) 15005–15010.
[36] S. Wunder, F. Polzer, Y. Lu, Y. Mei, M. Ballauff, J. Phys. Chem. C 114 (2010) 8814–8820.
[37] Y. Lu, Y. Mei, M. Ballauff, M. Drechsler, J. Phys. Chem. B 110 (2006) 3930–3937.
[38] S. Panigrahi, S. Basu, S. Praharaj, S. Pande, S. Jana, A. Pal, S.K. Ghosh, T. Pal, J. Phys. Chem. C 111 (2007) 4596–4605.
[39] Z. Zhang, C. Shao, P. Zou, P. Zhang, M. Zhang, J. Mu, Z. Guo, X. Li, C. Wang, Y. Liu, Chem. Commun. 47 (2011) 3906–3908.
[40] R. Han, X. Zhang, L. Wang, R. Dai, Y. Liu, Appl. Phys. Lett. 98 (2011) 221905.
[41] M. Murdoch, G.I.N. Waterhouse, M.A. Nadeem, J.B. Meterson, M.A. Keane, R.F. Howe, J. Lorca, H. Idriss, Nature Chem. 3 (2011) 489–492.
[42] Z.W. Seh, S. Liu, M. Low, S.-Y. Zhang, Z. Liu, A. Mlayah, M.-Y. Han, Adv. Mater. 24 (2012) 2310–2314.
[43] S.Y. Park, A.K.R. Lytton-Jean, B. Lee, S. Weigand, G.C. Schatz, C.A. Mirkin, Nature 451 (2008) 553–556.
[44] Z. Cheng, F. Nan, D. Yang, Y. Zhong, L. Ma, Z. Hao, L. Zhou, Q. Wang, Nanoscale 7 (2015) 1463–1470.
[45] S. Link, C. Burda, B. Nikoobakht, M.A. EI-Sayed, J. Phys. Chem. B 104 (2000) 6152–6163.
[46] X. Chen, Y. Chen, M. Yan, M. Qiu, ACS Nano 6 (2012) 2550–2557.
[47] A.O. Govorov, H.H. Richardson, Nano Today 2 (2007) 30–38.
[48] M. Hu, G.V. Hartland, J. Phys. Chem. B 106 (2002) 7029–7033.
[49] R. Loudon, J. Phys. A: Gen. Phys. 3 (1970) 233–245.
[50] M. Gratzel, A.J. Frank, J. Phys. Chem. 86 (1982) 2964–2967.
[51] K. Esumi, R. Isono, T. Yoshimura, Langmuir 20 (2004) 237–243.
[52] Y. Chang, D. Chen, J. Hazard. Mater. 165 (2009) 664–669.